ACCELERATED SPACE-TIME MODELING OF QUASI-LONGITUDINAL WAVES IN AUSTENITIC WELD STRUCTURES

Martin Spies and Michael Kröning
Fraunhofer-Institute for Nondestructive Testing (IZFP)
66123 Saarbrücken, Germany

INTRODUCTION

For ultrasonic inspection of austenitic welds and cladded components mostly horizontally polarized shear waves and quasi-longitudinal (qP) waves are applied. Depending on the testing situation the one or the other wave type offers certain benefits. To explain experimentally observed phenomena and to predict how qP-waves might be best employed, modeling of the respective wave propagation effects is useful. In this contribution, a computationally efficient modeling code is presented for qP-waves propagating in ideally fiber-textured austenitic weld material. Based on a mild anisotropy approximation given previously by Tverdokhlebov and Rose [1], a direct relationship between wave propagation directions and spatial coordinates has been obtained. This relationship has been applied to the Generalized Point-Source-Synthesis method (GPSS) to model radiation, propagation and scattering effects [2,3]. The GPSS-code thus improved is characterized by a considerable reduction of computer run-time and is therefore particularly convenient in view of a respective extension to inhomogeneous weldments. Numerical evaluations are presented for both continuous wave and time-dependent rf-impulse modeling for austenitic weld metal specimens, covering field profiles for a normal transducer and for a 32-element phased array probe. For the latter, wavefront images are also shown. The differences in the results obtained with this accelerated modeling code as compared with the exact code are of no practical importance. Further evaluations are shown in [4], where the calculation of three-dimensional transducer fields is considered.

PLANE WAVE RELATIONSHIPS

The plane wave solutions for a general transversely isotropic (TI) medium are obtained from the equation of motion for the displacement vector $\underline{u}$. Assuming time dependence $\sim e^{-j\omega t}$ - ω denoting the circular frequency - the solutions are in the form

$$\underline{u}_\alpha(\underline{R},\omega) = U\,\hat{\underline{u}}_\alpha \exp\left[j\,K_\alpha \hat{\underline{K}}\cdot\underline{R}\right], \tag{1}$$

Review of Progress in Quantitative Nondestructive Evaluation, Vol. 16
Edited by D.O. Thompson and D.E. Chimenti, Plenum Press, New York, 1997

where $\hat{\underline{K}}$ is the propagation direction. The determination of the polarization vectors $\hat{\underline{u}}_\alpha$ and the wave numbers K_α has been described in detail elsewhere [5]. It is

$$K_{SH}^2 = \varrho\omega^2 \Big/ \left(\mu_\perp + (\mu_\parallel - \mu_\perp)(\underline{a}\cdot\hat{\underline{K}})^2\right) , \tag{2}$$

$$K_{qSV,qP}^2 = 2\varrho\omega^2 \Big/ \left(B \mp (B^2 - 4A)^{\frac{1}{2}}\right) , \tag{3}$$

where A and B are functions of $\hat{\underline{K}}$ as well as of fiber direction $\underline{a}$ and the elastic constants. These are expressed by the generalized Lamé constants $\lambda_\parallel + 2\mu_\parallel$, $\lambda_\perp + 2\mu_\perp$, $\mu_\perp$, $\mu_\parallel$ and ν, which correspond to C_{11}, C_{33}, C_{44}, C_{66} and C_{13}. The decomposition into a pure transverse wave (SH: shear horizontal) and two quasi-waves (qSV: quasi-shear vertical, qP: quasi-pressure) is apparent from the polarization vectors, but is also evident from the dispersion relations: Eq. (2) contains only shear moduli, while in Eq. (3) all five elastic constants enter. Thus the quasi-waves are - apart from propagation into symmetry directions - neither pure transverse nor pure longitudinal waves.

QUASI-WAVE SPATIAL RELATIONSHIPS

In a lossless medium, the velocity of energy transport is given by the group velocity, which can be obtained according to

$$\underline{c}_\alpha = (\partial\omega(\underline{K})/\partial\underline{K})_{\underline{K}_\alpha} . \tag{4}$$

From Eqs. (2) and (3), one finds

$$\underline{c}_\alpha = v_\alpha \left(\hat{\underline{K}} + \mathcal{F}_\alpha\, (\underline{a}\cdot\hat{\underline{K}})(\underline{a} - (\underline{a}\cdot\hat{\underline{K}})\,\hat{\underline{K}})\right) , \tag{5}$$

where $v_\alpha = \omega/K_\alpha$ designates the phase velocity and where

$$\mathcal{F}_{SH} = (\mu_\parallel - \mu_\perp)\Big/(\mu_\perp + (\mu_\parallel - \mu_\perp)(\underline{a}\cdot\hat{\underline{K}})^2), \tag{6}$$

$$\mathcal{F}_{qSV,qP} = (2A)^{-1}\left(y_A + 2(\underline{a}\cdot\hat{\underline{K}})^2 z_A \pm \left(F_1 - (\underline{a}\cdot\hat{\underline{K}})^2 F_2\right)\Big/\sqrt{B^2 - 4A}\right) . \tag{7}$$

The quantities y_A, z_A, F_1 and F_2 depend on the elastic constants as given in Ref. [5]. Since the (energy) contribution to the wave field at an observation point $\underline{R}$ is characterized by group velocity, it follows for the respective unit vectors that

$$\hat{\underline{R}} = \hat{\underline{c}}_\alpha, \quad |\hat{\underline{R}}| = |\hat{\underline{c}}_\alpha| = 1 . \tag{8}$$

Thus it follows that

$$\hat{\underline{R}} = N_\alpha^{-1}\left(\hat{\underline{K}} + \mathcal{F}_\alpha\, (\underline{a}\cdot\hat{\underline{K}})(\underline{a} - (\underline{a}\cdot\hat{\underline{K}})\,\hat{\underline{K}})\right) , \tag{9}$$

$$(\underline{a}\cdot\hat{\underline{R}}) = N_\alpha^{-1}(\underline{a}\cdot\hat{\underline{K}})\left(1 + \mathcal{F}_\alpha(1 - (\underline{a}\cdot\hat{\underline{K}})^2)\right) , \tag{10}$$

$$N_\alpha = \left(1 + \mathcal{F}_\alpha^2\, (\underline{a}\cdot\hat{\underline{K}})^2(1 - (\underline{a}\cdot\hat{\underline{K}})^2)\right)^{1/2} . \tag{11}$$

A direct relationship between $\hat{\underline{K}}$ and $\hat{\underline{R}}$ can be derived from Eq. (9) for SH-waves [6], while - due to the complex structure of $\mathcal{F}_{qSV,qP}$ - this is not possible for the quasi-waves. However, approximative $\hat{\underline{K}}$-$\hat{\underline{R}}$-relationships can be obtained by making use of the elastic properties of the transversely isotropic weld structures under concern.

Mild Anisotropy Approximations

Following Tverdokhlebov and Rose [1], wave propagation in TI-weld metals can be considered applying a mild anisotropy approximation. Concentrating on the quasi-longitudinal wave, this fact will in the following be used to obtain 'simpler' expressions for $\mathcal{F}_{qP}$. Introducing

$$B_1 = 2\left(\nu + 2\mu_{\|} - (\lambda_\perp + 2\mu_\perp)\right) \;, B_2 = \lambda_{\|} + 2\mu_{\|} + \lambda_\perp + 2\mu_\perp - 2(\nu + 2\mu_{\|}) \tag{12}$$

and obeying that for austenitic steel $B_1 \cdot B_2, B_2 \cdot B_2 \ll \lambda_\perp + 2\mu_\perp$ allows to approximate

$$B^2 - 4A \;\cong\; \left(\lambda_\perp + 2\mu_\perp - \mu_{\|} + (\underline{\mathrm{a}} \cdot \hat{\underline{\mathrm{K}}})^2(B_1 - B_2) + 2(\underline{\mathrm{a}} \cdot \hat{\underline{\mathrm{K}}})^4 B_2\right)^2 \tag{13}$$

Hence, the following results:

- the 'K-approximation', originally proposed in [1], where insertion of (13) in (3) yields

$$K_{qP}^2 \;=\; \varrho\omega^2 \Big/ \left(\lambda_\perp + 2\mu_\perp + B_1(\underline{\mathrm{a}} \cdot \hat{\underline{\mathrm{K}}})^2 + B_2(\underline{\mathrm{a}} \cdot \hat{\underline{\mathrm{K}}})^4\right) \;; \tag{14}$$

  from (4) it then follows that

$$\mathcal{F}_{qP}^K = \frac{B_1 + 2B_2(\underline{\mathrm{a}} \cdot \hat{\underline{\mathrm{K}}})^2}{\lambda_\perp + 2\mu_\perp + B_1(\underline{\mathrm{a}} \cdot \hat{\underline{\mathrm{K}}})^2 + B_2(\underline{\mathrm{a}} \cdot \hat{\underline{\mathrm{K}}})^4} \;; \tag{15}$$

- the 'c-approximation', where (13) is directly applied to Eq. (5) to yield

$$\mathcal{F}_{qP}^c = \sum_{i=0}^{3} z_i(\underline{\mathrm{a}} \cdot \hat{\underline{\mathrm{K}}})^{2i} \Big/ \sum_{i=0}^{4} n_i(\underline{\mathrm{a}} \cdot \hat{\underline{\mathrm{K}}})^{2i} \tag{16}$$

  with respective coefficients n_i and z_i ([7]).

Resulting Polynomial Equations

Taking Eq. (10) to the square, introducing $X = x^2 \equiv (\underline{\mathrm{a}} \cdot \hat{\underline{\mathrm{K}}})^2$, $y^2 \equiv (\underline{\mathrm{a}} \cdot \hat{\underline{\mathrm{R}}})^2$ and using $\mathcal{F}_{qP}^K$ and $\mathcal{F}_{qP}^c$, respectively, leads to the polynomial equations

$$\mathcal{P}^K(X) \;=\; \sum_{i=0}^{5} a_i^K X^{5-i} = 0 \;, \tag{17}$$

$$\mathcal{P}^c(X) \;=\; \sum_{i=0}^{9} a_i^c X^{9-i} = 0 \;. \tag{18}$$

In (17), the coefficients a_i^K are given by

$$a_0^K \;=\; -(B_2)^2 \;, \tag{19}$$

$$a_1^K \;=\; (B_2)^2(4 - 3y^2) \;, \tag{20}$$

$$a_2^K \;=\; 2B_2(\lambda_\perp + 2\mu_\perp + B_1 - 2B_2) + 2y^2 B_2(2B_2 - B_1) \;, \tag{21}$$

$$a_3^K \;=\; -4B_2(\lambda_\perp + 2\mu_\perp + B_1) + 2y^2 B_2(\lambda_\perp + 2\mu_\perp + 2B_1) \;, \tag{22}$$

$$a_4^K \;=\; -(\lambda_\perp + 2\mu_\perp + B_1)^2 + y^2\left(2(\lambda_\perp + 2\mu_\perp)B_1 + (B_2)^2\right) \;, \tag{23}$$

$$a_5^K \;=\; y^2(\lambda_\perp + 2\mu_\perp)^2 \;, \tag{24}$$

while the a_i^c are more complicated functions of y^2 and the elastic constants [7].

Application of Newton's Method

The problem of finding the zeroes of $\mathcal{P}^K(X)$ and $\mathcal{P}^c(X)$ is solved by using Newton's method, which is - for polynomial equations - most efficient for numerical evaluation. Given a suitable initial approximation X_0, it is necessary to calculate

$$X_{m+1} = X_m - \mathcal{P}^{K,c}(X_m)/(\mathcal{P}^{K,c})'(X_m) \; , \tag{25}$$

for $m = 0, 1, 2, \ldots$. Applying the technique of synthetic division [8] allows to evaluate $\mathcal{P}^{K,c}(X_m)$ and $(\mathcal{P}^{K,c})'(X_m)$ without having to differentiate $\mathcal{P}^{K,c}(X_m)$ explicitly. With n designating the degree of the polynomial, Eq. (25) can be transformed into

$$X_{m+1} = X_m - b_n^{K,c}/c_{n-1}^{K,c} \; , \tag{26}$$

$$b_i^{K,c} = b_{i-1}^{K,c} X_m + a_i^{K,c} \; , \tag{27}$$

$$c_i^{K,c} = c_{i-1}^{K,c} X_m + b_i^{K,c} \; . \tag{28}$$

Starting with $X_0 = y^2$, the numerical evaluations performed in this study in general require three to four iterations to determine X with sufficient accuracy.

Direct $\hat{\underline{K}}$-$\hat{\underline{R}}$-Relationships

With the resulting solutions $(\underline{a} \cdot \hat{\underline{K}})^{K,c}$ of Eqs. (17) and (18), which are functions of $\hat{\underline{R}}$, the $\hat{\underline{K}}$-$\hat{\underline{R}}$-relationships follow from Eq. (9) according to

$$\hat{\underline{K}}^{K,c} = \left(1 - \mathcal{F}_{qP}^{K,c} \left((\underline{a} \cdot \hat{\underline{K}})^{K,c}\right)^2\right)^{-1} \left(N_{qP}^{K,c} \hat{\underline{R}} - \mathcal{F}_{qP}^{K,c} (\underline{a} \cdot \hat{\underline{K}}^{K,c})\, \underline{a}\right) \; . \tag{29}$$

Inserting (29) into Eq. (5) finally provides group velocity in dependence on the spatial coordinates $\hat{\underline{R}}$. The polarization vectors $\hat{\underline{u}}$ can be obtained in the same way, the respective expressions are omitted here.

ACCELERATED QP-MODELING CODE

Based on a theory of elastic wave propagation in TI-media [5], the Generalized Point-Source-Synthesis-method (GPSS) has been developed to model the radiation, propagation and scattering of elastic waves as generated by ultrasonic transducers in these media [2,3]. The physical background to the method is Huygens' principle: each point of a wave front is the starting point of an elementary wave, the new wave front is obtained as the superposition of all elementary waves. Applying the above results to the corresponding formulation (see Eq. (53) of Ref. [2]), the displacement vector describing the transducer-generated qP-wave field follows as

$$\underline{u}^{qP}(\underline{R}) = \sum_m \left\{ \hat{\underline{u}}(\widehat{\underline{R}_m^{\Delta}}) \cdot \frac{\exp\left(-\mathrm{j}\omega \, |\underline{R}_m^{\Delta}| \, / c_{qP}(\widehat{\underline{R}_m^{\Delta}})\right)}{|\underline{R}_m^{\Delta}|} \cdot \Gamma_{\text{point}}^{i\alpha}\left(\hat{\underline{K}}(\widehat{\underline{R}_m^{\Delta}})\right) \right\}, \tag{30}$$

where the dependence on fiber direction $\underline{a}$ is not explicitly expressed. It is $\underline{R}_m^{\Delta} = (\underline{R} - \underline{R}_m)$, $\widehat{\underline{R}_m^{\Delta}}$ is the corresponding unit vector and $\underline{R}_m$ designates the position

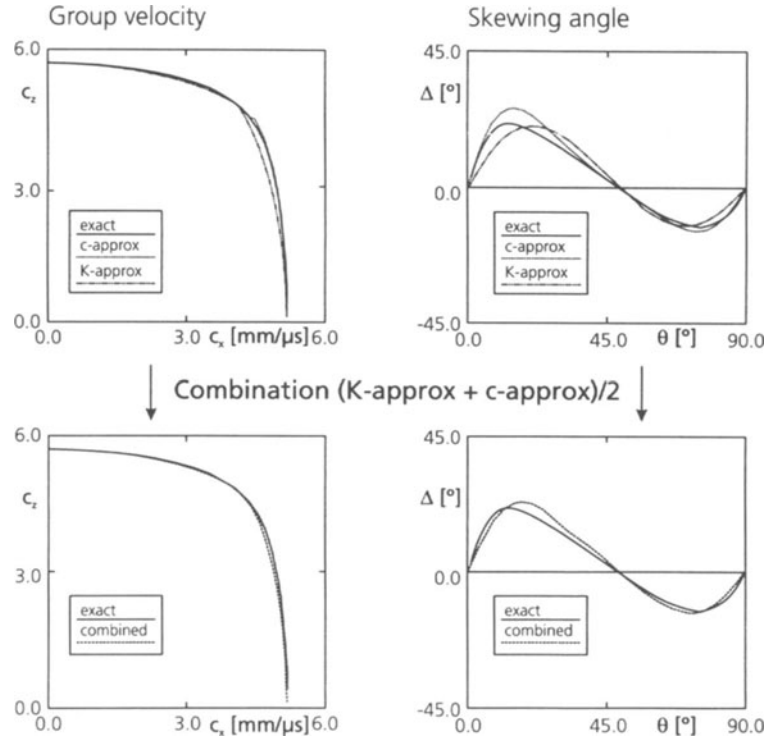

Figure 1. Comparison of approximations for group velocities and skewing angles. Elastic constants used are: $C_{11} = 217.1$ GPa, $C_{33} = 263.2$ GPa, $C_{44} = 82.4$ GPa, $C_{66} = 128.4$ GPa and $C_{13} = 144.4$ GPa.

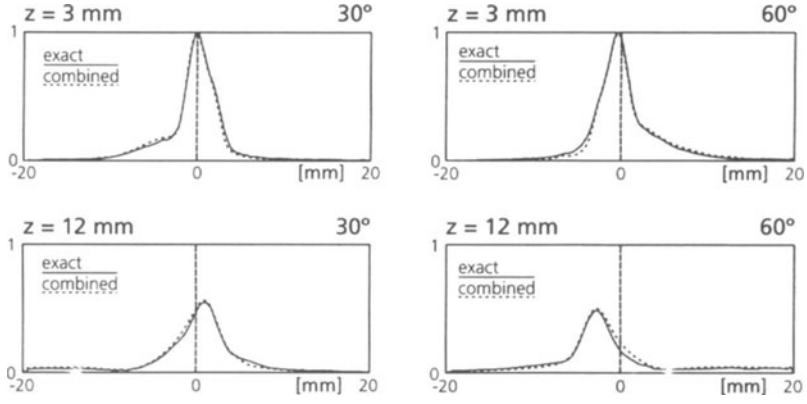

Figure 2. Field profile distributions at two distances z from the transducer in weld specimens with grains at 30° and 60° to the surface.

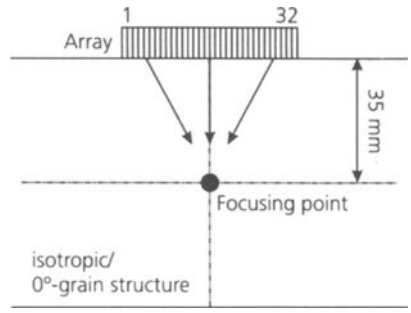

Figure 3. Modeling configuration: 32-element-array on top of a weld specimen. Point focusing is accomplished by time-delaying the single elements.

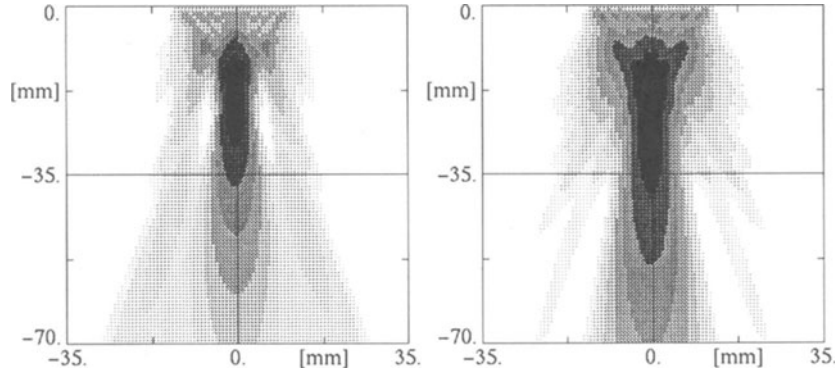

Figure 4. Field patterns resulting for the configuration shown in Fig. 3. Proper focusing requires adaption of the delay-times to the anisotropic structure. (Logarithmic scaling from 0 to -20 dB, in steps of 2.5 dB.)

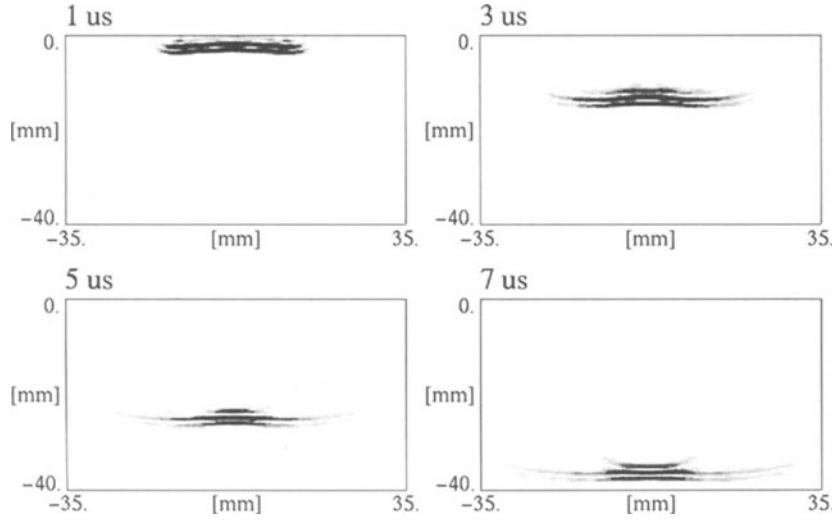

Figure 5. Wave front images at successive times. The energy focusing to 35 mm depth (7 μs) is clearly visible.

of the m-th tangential ($i=x, y$) or normal ($i=z$) point source. The determination of the directivities $\Gamma^{i\alpha}_{\text{point}}$ for arbitrarily oriented TI-media has been described in Ref. [2].

NUMERICAL EVALUATION

Numerical evaluation is performed in the x-z-plane for an ideally <100>-fiber-textured austenitic stainless steel (308), exhibiting transversely isotropic symmetry. Figure 1 shows the group velocity and skewing angle diagrams, where the exact and the approximated results are plotted. While group velocity is approximately calculated with only minor deviations from the exact results, the differences are larger for the skewing angles, mainly for angles of insonification between 0° and 45°. However, combining and averaging of the K- and c-approximations leads to better results, as also shown in Fig. 1.

This combined approximation has been applied to the GPSS-method for field pattern calculation for a longitudinal normal probe (6.3 mm diameter, 2.25 MHz frequency). Representatively, in Fig. 2 the field profile distributions are shown for two distances z from the transducer in weld specimens with grains at 30° and 60° to the surface. There are only small deviations of the combined approximation results from the exact calculation. Especially the relatively large deviations of about 15% in the skewing angles calculated for angles of insonification near 20° has no decisive effect on the GPSS-calculation. A fact, which is due the superposition of all wave contributions.

The savings in computer run-time make the optimized GPSS-code well suited for modeling of complex-structured transducers. As an example, a 32-element array probe (2.25 MHz, 26 x 12 mm^2) generating longitudinal waves is considered. The simulated situation is shown in Fig. 3: in a weld metal specimen with grains parallel to the surface, point focusing to a depth of 35 mm is achieved by correspondingly time-delaying the single elements. Figure 4 displays the field patterns calculated with the delay times for the isotropic base material and those adapted to the anisotropic grain structure. The corresponding wavefront images (Fig. 5) nicely illustrate the time-dependent rf-impulse modeling capabilities.

CONCLUSION

The derivation of a direct relationship between wave propagation directions and spatial coordinates using mild anisotropy approximations has been employed to obtain an optimized GPSS-modeling code for the quasi-pressure (qP) wave type in austenitic weld structures. While the modeling of quasi-wave propagation by 'conventional' GPSS, which has been validated previously [3], is based on a $\underline{c}$-$\underline{\hat{K}}$-look-up algorithm, the presented code is based on the fast numerical evaluation of an approximative $\underline{\hat{R}}$-$\underline{\hat{K}}$-relationship. Thus the computational efficiency of the method could even be improved: a reduction of computer run-time to about one third of GPSS-run-time has been achieved. From this point of view, the presented code seems particularly to be most convenient in view of an extension to inhomogeneous welds.

REFERENCES

1. A. Tverdokhlebov, J.L. Rose, "On Green's Functions for Elastic Waves in Anisotropic Media," J. Acoust. Soc. Am. 83, 118-121 (1988)
2. M. Spies, "Transducer-Modeling in General Transversely Isotropic Media Via Point-Source-Synthesis. Theory," J. Nondestr. Eval. 13, 85-99 (1994)

3. M. Spies, F. Walte, "Application-Directed Modeling of Radiation and Propagation of Elastic Waves in Anisotropic Media: GPSS and OPoSSM," in *Review of Progress in QNDE*, Vol. 14, eds. D.O. Thompson and D.E. Chimenti, Plenum Press, New York (1995), 1013-1020
4. M. Spies, N.K. Batra, K.E. Simmonds, R.B. Mignogna, "Numerical Modeling and Imaging of Three-Dimensional Transducer Fields in Anisotropic Materials," these proceedings
5. M. Spies, "Elastic Waves in Homogeneous and Layered Transversely Isotropic Media: Plane Waves and Gaussian Wave Packets. A General Approach," J. Acoust. Soc. Am. 95, 1748-1760 (1994)
6. M. Spies, M. Kröning, " A Computationally Efficient Modeling Code for SH-Wave Propagation in Austenitic Welds Using an Explicit Space-Time Green's Function," in *Review of Progress in QNDE*, Vol. 15, eds. D.O. Thompson and D.E. Chimenti, Plenum Press, New York (1996), 145-152
7. M. Spies, "Space-Time Modeling of Quasi-Waves in Austenitic Weld Structures," J. Nondestr. Eval., to be submitted
8. L.V. Atkinson, P.J. Harley, J.D. Hudson, *Numerical Methods with Fortran 77: A Practical Introduction*, Addison-Wesley (1989)